Journal of The Electrochemical Society

The Electrochemical Society
Advancing solid state & electrochemical science & technology

ACCEPTED MANUSCRIPT

The Influence of Electrode Constituents on Hydrogen Evolution Reaction on Phosphate W- and Mo-Bronze-Based Electrodes

To cite this article before publication: Maja Pagnacco *et al* 2022 *J. Electrochem. Soc.* in press https://doi.org/10.1149/1945-7111/ac96ab

Manuscript version: Accepted Manuscript

Accepted Manuscript is "the version of the article accepted for publication including all changes made as a result of the peer review process, and which may also include the addition to the article by IOP Publishing of a header, an article ID, a cover sheet and/or an 'Accepted Manuscript' watermark, but excluding any other editing, typesetting or other changes made by IOP Publishing and/or its licensors"

This Accepted Manuscript is **© 2022 The Author(s). Published by IOP Publishing Ltd.**.

This article can be copied and redistributed on non commercial subject and institutional repositories.

Although reasonable endeavours have been taken to obtain all necessary permissions from third parties to include their copyrighted content within this article, their full citation and copyright line may not be present in this Accepted Manuscript version. Before using any content from this article, please refer to the Version of Record on IOPscience once published for full citation and copyright details, as permissions will likely be required. All third party content is fully copyright protected, unless specifically stated otherwise in the figure caption in the Version of Record.

View the article online for updates and enhancements.

This content was downloaded from IP address 147.91.70.11 on 04/10/2022 at 09:19

The Influence of Electrode Constituents on Hydrogen Evolution Reaction on Phosphate W- and Mo-Bronze-Based Electrodes

Journal:	*Journal of The Electrochemical Society*
Manuscript ID	JES-108299.R1
Manuscript Type:	Research Paper
Date Submitted by the Author:	19-Sep-2022
Complete List of Authors:	Pagnacco, Maja; Institute of Chemistry Technology and Metallurgy Marković, Smilja; Institute of Technical Sciences of the Serbian Academy of Sciences and Arts Potočnik, Jelena; University of Belgrade Vinča Institute of Nuclear Sciences Krstić, Vesna; Mining and Metallurgy Institute Bor Tancic, Pavle; Geological Survey of Serbia, Geology Mojović, Miloš; University of Belgrade Faculty of Physical Chemistry Mojović, Zorica; Institut za hemiju tehnologiju i metalurgiju, Department for Catalysis and Chemical Engineering
Keywords:	phosphate tungsten bronze, phosphate molybdenum bronze, rhenium, hydrogen evolution reaction (HER), electrochemical activity

SCHOLARONE™
Manuscripts

Accepted Manuscript

The Influence of Electrode Constituents on Hydrogen Evolution Reaction on Phosphate W- and Mo-Bronze-Based Electrodes

Maja Pagnacco,[1] Smilja Marković,[2] Jelena Potočnik,[3] Vesna Krstić,[4] Pavle Tančić,[5] Miloš Mojović,[6] and Zorica Mojović[1,z]

[1]University of Belgrade, Institute of Chemistry, Technology and Metallurgy, Department for Catalysis and Chemical Engineering- National Institute of the Republic of Serbia, Njegoševa 12 11000 Belgrade, Serbia

[2]Institute of Technical Sciences of SASA, Belgrade, Serbia

[3]Vinča Institute of Nuclear Sciences – National Institute of the Republic of Serbia, University of Belgrade, Belgrade, Serbia

[4]Mining and Metallurgy Institute Bor, 19210 Bor, Serbia

[5]Geological Survey of Serbia, Rovinjska 12, 11000 Belgrade, Serbia

[6]University of Belgrade, Faculty of Physical Chemistry, Studentski trg 12-16, 11000 Belgrade, Serbia

[z]E-mail: zorica.mojovic@ihtm.bg.ac.rs

Abstract

Phosphate tungsten bronze (WPB) and phosphate molybdenum bronze (MoPB) were synthesized and modified with rhenium. The existing phases were established by X-ray powder diffraction (XRPD), electron paramagnetic spectroscopy (EPR) and Field emission scanning electron microscopy (FESEM). The electroactivity of bronze samples, with and without rhenium for hydrogen evolution reaction (HER) was tested. The influence of carbon black presence in the catalytic ink on the electrochemical activity was investigated. Collected results provide insight into the effects of the constituents of an electrode on its electrochemical activity.

Accepted Manuscript
For Review Only

Introduction

Harvesting hydrogen energy represents a sustainable and renewable alternative to fossil fuels [1]. Hydrogen evolution reaction (HER) has been widely investigated in order to achieve hydrogen production at an industrial scale with economical acceptability. The best-known HER electrocatalyst belongs to the platinum group metals. Platinum represents the state-of-the-art in this field [2], and the performance of new electrocatalysts is usually compared to the electroactivity of platinum under the same conditions. Due to the high cost and low abundance of platinum and the other elements from this group, new, more sustainable solutions are needed. The new electrocatalysts are developed with the aim to enable HER at lower overpotentials.

Tungsten oxide-based materials have been investigated as electrode materials for various applications [3-5], including the application for HER [6, 7]. These materials show good resistance to corrosion in acidic media, but their poor conductivity has to be improved [8] in order to achieve the needed efficiency for the HER process. Tungsten bronzes, as a type of tungsten oxide-based materials, have been investigated as electrode materials [9-12] as well. Additionally, the phenomenon of proton conductivity of heteropolyacid compounds (and their derivate, such as phosphate tungsten and molybdenum bronzes) has been recognized for many years, making these compounds known as superionic proton conductors at room temperature [13]. The phosphate bronzes show a metallic character due to delocalized electrons, making bronzes encouraging as a catalyst. The synergism between the oxide material and the active phase can be utilized to obtain a more efficient catalyst [14-15].

The effectiveness of electrocatalyst for HER depends on bonding energy employed in two successive and competitive processes: hydrogen adsorption and desorption. The hydrogen bonding strength of an efficient HER catalyst needs to be such to enable hydrogen bonding for the adsorption process and easy release of hydrogen in the next step. According to Trassati's volcano plot [16], rhenium has the required intermediate bonding energy value. So far, rhenium showed very low HER activity, but promising Re-intermetallic electrocatalysts have been investigated [17].

In this paper, the electrocatalysts based on phosphate tungsten bronze (WPB) and phosphate molybdenum bronze (MoPB) with and without added rhenium were investigated. The influence of carbon black on the efficiency of electrocatalyst for HER also was tested. The purpose of the

Accepted Manuscript
For Review Only

present work was to provide insight into the effects of the constituents of the electrode on its electrochemical activity.

Experimental

Bronzes –Re Synthesis

Phosphate tungsten bronze (WPB) is obtained by thermal treatment of 12-tungstophosporic heteropoly acid and its salt [18]. Namely, heteropoly acid hydrate $H_3PW_{12}O_{40}\times29\ H_2O$ (PWA) was obtained by dissolving 100 g $Na_2WO_4\times2H_2O$ (Carl Roth, Germany) in 100 ml distilled water, and an H_3PO_4-HCl (Merck) mixture and by extracting the precipitate with diethyl-ether (Carlo Erba, France) at room temperature. All used chemicals are P.A. grade. The dehydration process of $H_3PW_{12}O_{40}\times29\ H_2O$ (PWA) to $H_3PW_{12}O_{40}\times6\ H_2O$ (6-PWA) (yield of 6-PWA is about 30 g) is done by heating of PWA in a kiln at 80 °C. An aqueous solution of $H_3PW_{12}O_{40}\times6\ H_2O$ was then heated from room temperature (the velocity of heating is 10 °C min^{-1}), while thermal transformation (at 602 ºC) occurred and WPB was obtained. The sample is held in a furnace for 10 minutes at a 650 ºC temperature.

Phosphate molybdenum bronze (MoPB) is obtained in an identical way by thermal treatment of 12-molybdophosporic heteropoly acid and its salt [19]. For the bronzes synthesis freshly prepared heteropoly acids ($Na_2MoO_4\times2H_2O$, H_3PO_4-HCl mixture, all chemicals are P.A. grade) are used. The 442 ºC is the temperature for destroying the Keggin's anion and obtaining MoPB [20]. The heating rate was 10 °C min^{-1} and a sample was held in a furnace for 10 minutes at a particular temperature (500 ºC).

The incipient wetness impregnation method was used in order to obtain Re-bronze material. The bronze samples were heated up to 350 °C in order to remove adsorbed water and cooled to room temperature in a dry atmosphere before the solution of sodium perrhenate was added. The samples were then dried at 90 °C to evaporate solvent and calcined at 350 °C for 1 h in air. The amount of rhenium introduced in this manner was 100 mg Re per 1 g of bronze. $NaReO_4$ was calcined under the same conditions.

Particle size distribution

Accepted Manuscript For Review Only

The particle size distribution in water suspensions was determined by a laser light-scattering particle size analyzer (PSA) (Mastersizer 2000; Malvern Instruments Ltd., Malvern, Worchestershire, U.K.). Prior to measurement, the WPB and MoPB powders were dispersed in distilled water, using an ultrasonic bath, for 5 min. The measurements were done in a dynamic condition with a pump rotation of 1100 rpm.

X-ray powder diffraction (XRPD)

The X-ray powder diffraction (XRPD) patterns of MoPB, WPB, Re-MoPB and Re-WPB were obtained using a Rigaku Ultima4 automated diffractometer with a Cu tube operated at 40 kV and 40 mA. The instrument was equipped with a curved graphite monochromatic diffraction beam and Xe-filled proportional counter. The diffraction data were collected in the 2θ Bragg angle ranges from 3º to 140º, counting for 0.6 seconds at every 0.02º step. The divergence and receiving slits were fixed at 0.5º and 0.15 mm, respectively. The XRPD measurements were performed ex-situ at room temperature in a stationary sample holder. Diffractometer alignment was checked by means of a standard Si powder material.

Calculations of the unit cell dimensions were accomplished with the LSUCRI program [21]. Additionally, the tetragonal sodium perrhenate ($NaReO_4$ [22]) was used as an internal standard for the aforementioned calculations.

Electron Paramagnetic Resonance (EPR)

The electron paramagnetic resonance (EPR) spectra of the powder samples were recorded at room temperature by a Bruker Elexsys II E540 spectrometer operating at X-band (9.5 GHz) with the following settings: modulation amplitude 2 G; modulation frequency 100 kHz; microwave power 6.3 mW; scan range 514 mT. The spectra were recorded and analyzed using the Xepr software (Bruker BioSpin Germany).

Field emission scanning electron microscopy (FESEM)

The samples' morphology and chemical composition were investigated by field emission scanning electron microscopy equipped with an energy dispersive X-ray spectrometer (FESEM-EDS, FEI

Accepted Manuscript
For Review Only

SCIOS 2 Dual Beam). The samples were recorded under a high vacuum with an acceleration voltage of 10 kV. EDS elemental mapping was performed at 20 kV and 250x magnification, while the acquisition time was 40 min. Prior to analysis, the samples were sputter-coated with Au in order to improve the conductivity of the samples.

Electrochemical measurements

The electrochemical activity of starting bronze and Re-bronze samples was investigated using an Autolab PGSTAT302N (Metrohm-Autolab BV, Netherlands) and three-electrode cell with reference electrode Ag/AgCl in 3 M KCl, a platinum rod as a counter electrode and a glassy carbon electrode (GCE, diameter of 3 mm) coated with the catalyst as the working electrode. The GCE was polished with alumina powder and sonicate in distilled water and ethanol prior to the application of catalyst ink. A catalyst ink was prepared by sonicating 20 mg of the bronze powder (starting bronze or Re-bronze) in a mixture of 1 ml of isopropyl alcohol and 100 µl of 5 wt. % Nafion solution. 5 µl of prepared ink was applied on the surface of GCE. After evaporation, the loading of catalyst on GCE was 1.3 mg cm^{-2}, and the electrodes were designated as WPB, MoPB, Re-WPB and Re-MoPB.

Alternatively, the ink was prepared with the addition of carbon black (Vulcan, XC 72) in the amount of 10 wt.% of bronze and the modified GC electrodes were designated as WPB-C, MoPB-C, Re-WPB-C and Re-MoPB-C.

The geometric surface area of the electrode (0.0706 cm^2) was used for the calculation of current density.

Results and Discussion

Particle size distribution results

The particle size distribution based on number with inserted characteristic values of d(0.1), d(0.5), d(0.9) and *span*, for WPB and MoPB are presented in **Fig.1a** and **1b** respectively.

Figure 1.

As it can be seen, WPB and MoPB have very similar size distribution, with average particle size of 0.241 and 0.275 µm, respectively.

Accepted Manuscript For Review Only

XRPD results

It was determined that the XRPD pattern of MoPB (**Fig.2a**; **Table 1**) is iso-structural with the orthorhombic molybdite (MoO_3 [23]), and also adequate to the orthorhombic low- and high-$P_{0.18}Mo_{4.000}O_{12.66}$ phases synthesized above 440 ºC [19]. In the case where sodium perrhenate was added **(**Re-MoPB; **Fig.2b**), it was determined that this sample consists of clearly distinguishable two different phases, i.e. MoPB (~84 %) and $NaReO_4$ (~16 %). Differences between these phases are also more or less visible from the comparative presentations within the magnified 2θ angle areas (**Figs. 2c** and **2d**). For example, the Re-MoPB phase is with smaller observed intensities and observed 2θ angles in comparison with the MoPB phase.

Figure 2.

Calculated unit-cell parameters of MoPB and Re-MoPB are quite smaller than those for MoO_3 (**Table 1**).

Table 1.

Although the ionic radius of Re^{6+} is something smaller than Mo^{6+} (0.55Å and 0.59Å, respectively, in coordination VI [24]), the Re-MoPB phase is characterized by larger observed inter-planar spacings and unit-cell parameters than MoPB. Such a fact further strongly indicates that some part of Re enters into the structure of MoPB. This is not much surprising, because our previous studies of Li- and Ca-doped phosphate tungsten bronzes showed that unit-cell parameters could expand by adding considerably smaller Li^+ ions in larger amounts [25] or even compress by adding considerably larger Ca^{2+} ions [26]. Furthermore, it seems that entering Re into the MoPB increase its structure ordering, due to the smaller estimated standard deviations (esd's) of Re-MoPB in comparison with the MoPB phase (**Table 1**).

On the other hand, it was determined that the WPB phase (**Fig.3a**; **Table 2**) is adequate to the monoclinic PW_8O_{26} phase synthesized at 750 ºC [18], which is structurally very different from the MoPB (**Fig.2a**). In the case were sodium perrhenate was added **(**Re-WPB; **Fig.3b**), it was determined that this sample also consists of two clearly distinguishable different phases, i.e. WPB (~76 %) and $NaReO_4$ (~24 %).

Accepted Manuscript
For Review Only

Figure 3.

Calculated unit-cell parameters of WPB and Re-WPB are mutually very similar to each other (**Table 2**).

Table 2.

Therefore, those cannot be used as reliable evidence that Re^{6+} replaced W^{6+} (ionic radius ratios of 0.55Å and 0.60Å, respectively, in coordination VI [24], or that Re enters into the Re-WPB structure in any other forms. However, there are three noticeable facts that could reasonably testify to the opposite conclusion: 1. the observed inter-planar spacings of the Re-WPB phase are increased in comparison with WPB (**Table 2**), similarly to the MoPB and Re-MoPB samples (**Table 1**); 2. Re-WPB phase is observed with smaller intensities and 2θ angles in comparison to the WPB phase (**Fig.3c** and **3d**), similarly to the MoPB and Re-MoPB samples (**Figs.2c** and **2d**); and 3. Quantity of the sodium perrhenate is in the Re-WPB in fewer amounts than in Re-MoPB for about 50% (**Figs.2** and **3**; **Tables 1** and **2**), further indicating that Re enters even in a larger amount in the Re-WPB phase than in the Re-MoPB. Finally, significantly large esd's of both WPB and Re-WPB phases (**Table 2**) could also indicate their higher structure disordering.

EPR measurements

The electron paramagnetic resonance (EPR) technique was employed to assess the structural and electronic properties of the investigated samples. The EPR spectra of MoPB and rhenium-modified bronze (**Fig.4a** and **4b**) showed the greatest difference.

Figure 4.

The sharp peak at g = 1.939 of MoPB spectra can be assigned to paramagnetic Mo^{5+} centers [27]. At the EPR spectrum of Re-MoPB, the peak was shifted to the position at g = 2.150 with the intensity increased around 100 times. This peak can be assigned to the Mo^{6+}-O_2^- complex [28]

Accepted Manuscript
For Review Only

formed at the position of reduced metal site or oxygen vacancy. Furthermore, the EPR signal intensity and shape, which are related to the number of spins and the type of paramagnetic centers, indicated that the incorporation of Re into the cell structure of MoPB enabled increased accessibility of oxygen to the structure resulting in the appearance of a new type of paramagnetic entity. Besides, the formation of high spin multiplets at g=4 was also noticed (**Fig. 4b**). We presume that these peaks can be assigned to the formation of the Mo^{4+}-Re complex. Similar behavior was noticed for molybdenum-copper complex compounds [29].

The EPR spectra of WPB and Re-WPB, recorded under the same conditions, have shown no EPR signal (spectra not presented). Although it can be expected that complexes similar to those in Mo bronze were formed, since W^{6+} is silent [30], it was impossible to confirm obtained structure by the EPR.

FESEM results

Morphological studies of bronze and Re-modified bronze samples were performed using field emission scanning electron microscopy and the obtained micrographs are presented in **Fig.5**. It is evident that the samples are composed of plate-like structures which are more clearly defined in the MoPB sample (**Fig.5a**). The modification with Re resulted in greater aggregation of particles for Re-MoPB sample (**Fig.5b**). In the case of WPB sample (**Fig.5c**) a higher degree of particle agglomeration is visible, while the addition of Re did not cause significant changes in sample morphology.

Figure 5.

In order to confirm the chemical composition and homogeneity of investigated samples, EDS elemental mapping was performed and the obtained results are shown in **Fig.6**, together with the corresponding spectra (range from 0.1 – 12 keV is given for the sake of clarity). To visually indicate the presence of distinct elements, different colors were used. Carbon (C) is displayed in red, oxygen (O) in green and phosphorus (P) in blue on all maps, whereas molybdenum (Mo) is shown in yellow (**Fig.6a** and **6c**), tungsten (W) in grey (**Fig.6e** and **6g**) and rhenium (Re in light blue (**Fig.6c** and **6g**) color. The obtained maps reveal that Re was

Accepted Manuscript
For Review Only

homogeneously distributed over the specimen in both modified bronze. Peaks for obtained elements are visible in the corresponding spectra.

Figure 6.

Electrochemical measurements

The electrochemical performance of bronze-modified GCE in 0.5 M H_2SO_4 was studied by cyclic voltammetry (CV), linear sweep voltammetry (LSV) and electrochemical impedance spectroscopy (EIS).

Cyclic voltammograms of molybdenum bronze material (**Fig.7a**) showed that the addition of carbon black to the electrode composition showed the highest enhancement of current response, even better than the addition of rhenium and carbon black combined. The addition of rhenium to MoPB did not have a significant influence on the electrode activity. Molybdenum bronze electrodes were prone to corrosion in 0.5 M H_2SO_4 as can be seen in the inset of **Fig.7a**, where the first four cycles recorded for MoPB-C electrode are presented. Two characteristic pairs of peaks of molybdenum oxides in acidic media can be seen at voltammograms of electrodes where carbon was added. The pair A1/C1 is ascribed to the insertion of hydrogen in the molybdenum oxide matrix, while pair A2/C2 is ascribed to the reduction of Mo(VI) to a lower oxidation state [31, 32]. The same peaks can be seen at the voltammogram of Re-MoPB-C, but the currents were significantly reduced. Rhenium probably interacted with molybdenum during the impregnation/calcination procedure forming the complexes seen at the EPR spectra.

Figure 7.

A cyclic voltammogram of tungsten bronze material (**Fig.7b**) also showed the remarkable enhancing effect of adding carbon black. However, the addition of rhenium had a similar effect, while the addition of carbon black to the electrode that contained rhenium did not show any further enhancement. The electrodes based on tungsten were stable, without expressed corrosion behavior (inset in **Fig.7b**). On the contrary, a slight increase in current was noticed with cycling that can be attributed to the conversion of surface hydroxide to oxides [33, 34]. The features of recorded

Accepted Manuscript
For Review Only

voltammograms are consistent with the previously published data indicating H^+-intercalation in tungsten oxide structure [35, 36].

It is worth noting that the catalytic system based on Re-WPB showed much higher capacitive currents in comparison to the WPB, and also to MoPB and Re-MoPB systems. The observed difference in the shape of cyclic voltammograms can be ascribed to the combined effect of the capacitance originating from the formation of the electrical double layer and the pseudocapacitance [37]. The synergetic effect between rhenium and bronze, obtained for the WPB sample, but absent for the MoPB sample, is probably the consequence of their different structures. According to the XRPD analysis, the incorporation of Re in MoPB led to the ordering of the structure and probably to the voltammetric inaccessibility of Re species. On the other hand, the incorporation of Re to the WPB resulted in a disordered structure with more accessible Re specie

HER activity of GCE modified with investigated bronze samples was assessed using linear sweep voltammetry. LSV plots of investigated bronze samples were recorded at a scan rate of 5 mV s^{-1} are presented in **Fig.8a** and **8c**. s.

Figure 8.

An overpotential of 605 mV and 571 mV (vs. Ag/AgCl) was measured to obtain 10 mA cm^{-2} with MoPB-C and Re-MoPB-C. The activity of MoPB and Re-MoPB was too low to reach the desired value current density in a reasonable potential range. The addition of rhenium to molybdenum bronze increased the activity of bronze, but not to a significant degree. Commercial molybdenum oxide achieves the standard current density of 10 mA cm^{-2} at an overpotential of 220 mV (vs. RHE) [38]. The tungsten-based samples reached 10 mA cm^{-2} at an overpotential of 754 mV, 659 mV, 576 mV and 462 mV (vs. Ag/AgCl) for WPB, WPB-C, Re-WPB and Re-WPB-C, respectively. The addition of carbon black lowered the overpotential for 95 mV while the addition of rhenium contributed to the lowering of the overpotential for 178 mV in comparison to the starting tungsten bronze sample. The addition of carbon black to the Re-containing tungsten bronze sample contributed to further lowering of overpotential for another 114 mV. The overpotential of tungsten oxide for HER significantly depends on the structure of the oxide material [39].

Tafel slopes were derived from LSV plots compensated for iR drop [40] using resistance value, R_s, obtained from EIS measurements. Tafel slopes (**Fig.8b** and 8**d**) were significantly

Accepted Manuscript
For Review Only

increased by the addition of rhenium to both bronze materials while adding carbon black contributed to its lowering. Tafel slopes obtained for WPB and WPB-C electrodes were close to the values of 120 mV dec^{-1} expected for the Volmer step (i.e. discharge reaction) as the rate-determining step [41]. The values of Tafel slopes for molybdenum-based samples were significantly higher than the values expected for HER process (30, 40 and 120 mV dec^{-1}) and could not be explained with simple Volmer-Tafel-Heyrovsky steps [42]. The region of linearity on the Tafel plot was increased for both Mo- and W-based bronze with added rhenium. It amounted to 400 mV for Re-MoPB and 300 mV for Re-WPB. The presence of the rhenium enabled the hydrogen evolution reaction to start at lower potentials. However, it seems that rhenium also increased the energy of the electrode-hydrogen bond causing the increase in the Tafel slope. A more negative potential was needed to be reached in order for hydrogen molecules to be formed in the next step. The addition of carbon black to Re-containing bronze samples resulted in decreased Tafel slope and narrowed linear region. Tafel analysis showed that the introduction of rhenium in the bronze structure resulted in a similar response for both bronze samples. This finding indicates that the primary site for hydrogen evolution was the formed rhenium-bronze complex, rather than bronze or $NaReO_4$. A similar result was obtained by Schrebler [43] who investigated the HER on a rhenized-Au electrode and found out that HER occurred preferentially on the electrodeposited rhenium rather than on the Au surface. Furthermore, Schrebler stated that Re-H species were formed. We can suppose a similar occurrence and that would explain the broader Tafel region, i.e. more difficult formation of the hydrogen molecule and its release.

Electrochemical impedance spectroscopy (EIS) was performed at onset potentials for HER determined from LSV curves using the tangent method. The recorded Nyquist plots are presented in **Fig.9a** and **9b**.

Figure 9.

Nyquist plots of Mo-based electrodes showed an inductive loop at low frequencies. The inductive behavior shows that the electric field that opposes the applied electric field was formed. This kind of behavior is usually associated with intermediate corrosion products adsorbed on the electrode surface [44, 45] or with the changed properties of the oxide layer caused due to ion migration [46]. Since Mo-based materials showed corrosive behavior the most probable reason

Accepted Manuscript For Review Only

was changed surface properties at the applied potential. This kind of behavior was not noticed in Nyquist plots of W-based electrodes confirming their stability at the applied potential.

All recorded Nyquist plots exhibited the depressed semicircle indicative of the inhomogeneity of the electrode surface. The constant phase element (CPE) is usually used instead of the capacitance in the equivalent electric circuits to accommodate this feature. The impedance of CPE is given as:

$$Z = \frac{1}{Y} = \frac{1}{(i\omega)^n Q} \qquad (1)$$

where Y is CPE admittance, i is the imaginary unit, ω is the angular frequency, n is the CPE exponent which is associated with the system inhomogeneity and Q has the numerical value of the admittance (1/ |Z|) at ω = 1 rad/s.

The capacitance element CPE will become the pure capacitance, pure resistance, and Warburg impedance when $n = 1$, $n = 0$, and $n = 0.5$, respectively.

The addition of Re to W-based bronze resulted in a Nyquist plot with two semicircles. Therefore, the obtained experimental data of Re containing WPB samples were fitted with two equivalent circuits (**Fig.9c**) and the obtained results are presented in **Table 3**.

Table 3.

The equivalent circuit A consists of an internal resistance R_s in a series combination with a parallel R_{ct}-CPE circuit where R_{ct} component is related to the faradic process, while the CPE component is related to the electrode-electrolyte interfacial properties. Circuit B consists of an internal resistance R_s in a series combination with parallel R_{ct}-CPE circuits with embedded second parallel R_{ct}-CPE. This circuit was used to fit experimental EIS data for Re-WPB and Re-WPB-C samples in order to accommodate two semicircles that appeared in Nyquist plots.

The value charge transfer resistance recorded for WPB was significantly lower than the value recorded for MoPB. The addition of rhenium to bronze resulted in a decrease in the charge transfer resistance. W-based samples with Re showed a Nyquist plot with two semicircles which implies the existence of two phases in contact with the electrolyte [47]. This result is in accordance with the result of XRD characterization which implied that Re-WPB sample contained more

Accepted Manuscript
For Review Only

incorporated rhenium than Re-MoPB sample. The value of ohmic resistance was significantly lower for the electrodes containing carbon in comparison to the electrodes without it.

Conclusion

Two samples of phosphate bronze material, tungsten type and molybdenum type were synthesized. The same particle size distribution was found for both bronzes, excluding this as a possible factor that can affect the outcome of modification of these samples with rhenium. Rhenium modification was performed by sodium perrhenate under elevated temperatures. XRPD analysis confirmed the presence of the $NaReO_4$ phase in both Re-containing samples. The incorporation of Re in bronze structure was more prominent for tungsten phosphate bronze. EPR measurements clearly indicated the interaction of incorporated Re with MoPB structure. This confirmation could not be obtained for the Re-WPB sample due to the EPR-silent nature of the tungsten-based sample. Cyclic voltammetry analysis in 0.5M H_2SO_4 showed that WPB samples are more stable in this environment than MoPB samples. Overpotential for HER and Tafel slopes obtained from LSV measurements showed that the presence of Re was beneficial, but that the presence of carbon in the final ink was of crucial importance for the electrode efficiency. ESI measurements showed that the presence of Re in the WPB sample resulted in the formation of two phases, while that result was not obtained for the MoPB sample.

Acknowledgment

This work was supported by the Ministry for Education, Science and Technological Development of the Republic of Serbia (Grants No. 451-03-68/2022-14/200026 and 451-03-68/2022-14/200175). We would like to acknowledge dr. Zoran Nedić for the assistance in bronze preparation.

References

[1] M. Zeng and Y. Li, *J. Mat. Chem. A*, **3**, 14942 (2015).

[2] J. K. Norskov, T. Bligaard, A. Logadottir, J. R. Kitchin, J. G. Chen, S. Pandelov and J. K. Norskov, *J. Electrochem. Soc.*, **152**, J23 (2005).

[3] H. Quan, Y. Gao and W. Wang, *Inorg. Chem. Front.*, **7**, 817, (2020).

[4] P. A. Shinde and S. C. Jun, *ChemSusChem*, **13**, 11 (2020).

[5] Y. Zhou, X. Hub, Y. Xiao and Q. Shu, *Electrochim. Acta*, **111**, 588 (2013).

Accepted Manuscript For Review Only

[6] T. H. Wondimu, A. W. Bayeh, D. M. Kabtamu, Q. Xu, P. Leung and A. A. Shah, *Int. J. Hydrog. Energy*, **47**, 20378 (2022).

[7] A. K. Nayak, M. Verma, Y. Sohn, P. A. Deshpande and D. Pradhan, A*CS Omega*, **2**, 7039 (2017).

[8] H. Tian, X. Cui, L. Zeng, L. Su, Y. Song and J. Shi, *J. Mater. Chem. A*, **7**, 6285 (2019).

[9] D. B. Šepa, D. S. Ovcin and M. V. Vojnović, *J. Electrochem. Soc.* **119**, 1285 (1972).

[10] J. Vondrák and J. Balej, *Electrochim. Acta*, **18**, 1017 (1973).

[11] J. Vondrák and J. Balej, *Electrochim. Acta*, **20**, 283 (1975).

[12] J. P. Kandin, A. K. Vijh and A. B. Chughtai, *J. Electrochem. Soc.*, **120**, 1174 (1973).

[13] O. Nakamura, T. Ogino, T. Kodoma, *Solid State Ion.*, **3**, 347 (1981).

[14] A. I. Onuchukwu, J. Electrochem. Soc. **130**, 1077 (1983).

[15] O. L. Semerikova, S. V. Vakarin, A. V. Kosov, S. V. Plaksin, A. A. Pankratov, O. V. Grishenkova, Y. P. Zaykov, A. B. Shishmakov, Y. V. Mikushina and L. A. Petrov, *J. Electrochem. Soc.*, **166**, D792 (2019).

[16] S. Trasatti, *J. Electroanal. Chem.*, **39**, 163 (1972).

[17] L. Dan and N.-T. Suen, *Eur. J. Inorg. Chem.*, **2021**, 4085 (2021).

[18] U. B. Mioč, R. Ž. Dimitrijević, M. Davidović, Z. P. Nedić and M. M. Mitrović, *J. Mater. Sci.*, **29**, 3705 (1994).

[19] R. Ž. Dimitrijević, Ph. Colomban, U. B. Mioč, Z. P. Nedić, M. R. Todorović, N. Tjapkin and M. Davidović, *Solid State Ion.*, **77**, 250 (1995).

[20] M. C. Pagnacco, J. P. Maksimović, T. M. Mudrinić, Z. D. Mojović and Z. P. Nedić, *J. Electroanal. Chem.,* **849**, 113369 (2019).

[21] R. Garvey, *Least-square unit cell refinement,* Version 86.2, Dept. of Chemistry, North Dakota State University (1987)

[22] ICDD-PDF 35-0828, Sodium perrhenate, $NaReO_4$, National Bureau of Standards (U.S.), Monogr. 25, 21, 119 (1984).

[23] ICDD-PDF 5-0508, Molybdite syn, MoO_3, Swanson, Fuyat, National Bureau of Standards (U.S.), Circ 539, III, 30 (1954).

[24] R. D. Shannon, *Acta Crystallogr*. **A32**, 751 (1976).

[25] M. Vujković, Z. Nedić, P. Tančić, O. S. Aleksić, M.V. Nikolić, U. Mioč and S. Mentus, *J. Mater. Sci.*, **51**, 2481 (2016).

Accepted Manuscript
For Review Only

[26] T. V. Maksimović, J. P. Maksimović, P. I. Tančić, N. I. Potkonjak, Z. P. Nedić, Lj. G. Joksović and M. C. Pagnacco, *Sci.Sinter.*, **53**, 223 (2021).

[27] R. B. Watson and U. S. Ozkan, *J. Phys. Chem. B*, **106**, 6930 (2002).

[28] X. Tan, L. Wang, C. Cheng, X. Yan, B. Shen and J. Zhang, *Chem. Commun.*, **52**, 2893 (2016).

[29] N. Bridonneau, P. Quatremare, H. J. von Bardeleben, J-L. Cantin, S. Pillet, El-E. Bendeif and V. Marvaud, *Eur. J. Inorg. Chem.*, **3-4**, 370 (2018).

[30] A. Punnoose and M. S. Seehra, *Catal. Lett.*, **78**, 157 (2002).

[31] W. Baoxing and D. Shaojun, *J. Electroanal. Chem.*, **379**, 207 (1994).

[32] V. S. Saji and C-W. Lee, *ChemSusChem*, **5**, 1146 (2012).

[33] H. Wang, D. Kong,P. Johanes, J. J. Cha, G. Zheng, K. Yan, N. Liu and Y. Cui, *Nano Lett.*, **13**, 3426 (2013).

[34] A. K. Nayak, M. Verma, Y. Sohn, P. A. Deshpande and D. Pradhan, *ACS Omega*. **2**, 7039 (2017).

[35] L. H. M. Krings and W. Talen, *Sol. Energy Mater. Sol. Cells*, **54**, 27 (1998).

[36] W. Cheng, E. Baudrin, B. Dunn and J. I. Zink, *J. Mater. Chem.*, **11**, 92 (2001).

[37] N. A. Samsudin, Z. Zainal, H. N. Lim, Y. Sulaiman, S-K. Chang, Y-C. Lim, A. K. Ayalae and W. N. M. Amin, RSC Adv., 8, 23040 (2018).

[38] F. Haque, A. Zavabeti, B. Y. Zhang, R. S. Datta, Y. Yin, Z. Yi, Y. Wang, N. Mahmood, N. Pillai, N. Syed, H. Khan, A. Jannat, N. Wang, N. Medhekar, K. Kalantar-zadeh and J. Z. Ou, *J. Mater. Chem. A*, **7**, 257 (2019).

[39] Y. Li, X. Zhai, Y. Liu, H. Wei, J. Ma, M. Chen, X. Liu, W. Zhang, G Wang, F. Ren and S. Wei, *Front. Mater.*, **7**, 105 (2020).

[40] S. Anantharaj, S. Noda, M. Driess and P. W. Menezes, *ACS Energy Lett.*, **6**, 1607 (2021).

[41] Y. Shen, L. Li, J. Xi and X. Qiu, *J. Mater. Chem. A*, **4**, 5817 (2016).

[42] A. Morozan, V. Goellner, Y. Nedellec, J. Hannauer and F. Jaouen, *J. Electrochem. Soc.*, **162**, H719 (2015).

[43] R. Schrebler, P. Cury, M. Orellana, H. Gomez, R. Cordova and E.A. Dalchiele, *Electrochim. Acta*, **46**, 4309 (2001).

[44] I. Pivac and F. Barbir, *J. Power Sources*, **326** 112 (2016).

[45] M. P. Gomes, I. Costa, N. Pébère, J. L. Rossi, B. Tribollet and V. Vivier, *Electrochim. Acta*,

Accepted Manuscript
For Review Only

306, 61 (2019).

[46] S. Taibl, G. Fafilek and J. Fleig, *Nanoscale*, **8**, 13954 (2016).

[47] A. R. C. Bredar, A. L. Chown, A. R. Burton and B. H. Farnum, *ACS Appl. Energy Mater.*, **3**, 66 (2020).

Accepted Manuscript

For Review Only

Figure captions

Figure 1. Particle size distribution based on number for a) WPB and b) MoPB.

Figure 2. XRPD patterns of: (a) MoPB; (b) Re-MoPB; Magnified 2θ angle area (c) from 9º to 42º and d) from 42º to 80º of the comparative presentation of the studied MoPB (blue color) and Re-MoPB (red color) phases. Note: The reflection positions of the orthorhombic MoO_3 phase [23] are represented by black vertical tick marks, whereas the reflection positions of the tetragonal $NaReO_4$ phase [22] are represented by green vertical tick marks.

Figure 3. XRPD patterns of: (a) WPB; (b) Re-WPB. Magnified 2θ angle area (c) from 15º to 42º and d) from 42º to 80º of the comparative presentation of the studied WPB (blue color) and Re-WPB (red color) phases. Note: The reflection positions of the monoclinic PW_8O_{26} phase [18] are represented by black vertical tick marks, whereas the reflection positions of the tetragonal $NaReO_4$ phase [22] are represented by green vertical tick marks.

Figure 4. EPR spectra of a) MoPB and Re-MoPB; b) enlarged part of spectra a).

Figure 5. FESEM micrographs of a) MoPB, b) Re-MoPB, c) WPB and d) Re-WPB.

Figure 6. The elemental maps from the whole area shown in the FESEM image and corresponding spectrum for MoPB (a and b), WPB (c and d), Re-WPB (e and f) and Re-MoPB (g and h) samples.

Figure 7. 5th cyclic voltammogram recorded in 0.5 M H_2SO_4 at a scan rate of 100 mVs^{-1} on a) molybdenum bronze modified GCE (inset: cycling of MoPB-C; the arrow indicates the direction of increasing cycle number) and b) tungsten bronze modified GCE (inset: cycling of Re-WPB-C).

Figure 8. iR-corrected linear sweep voltammetry recorded in 0.5 M H_2SO_4 at scan rate of 5 mVs^{-1} and corresponding Tafel slopes for molybdenum bronze electrodes (a and b) and tungsten bronze electrodes (c and d).

Figure 9. Nyquist plot recorded at onset potential of HER on molybdenum bronze (a) and tungsten bronze-based (b) electrodes in 0.5 M H_2SO_4; c) The equivalent electric circuits used to fit EIS data.

Accepted Manuscript
For Review Only

Table 1. Observed inter-planar spacings (d_{obs}, in Å) and intensities (I_{obs}, in %) of MoPB and Re-MoPB compared to the reference MoO_3 with their adequate Miller's hkl indices presented [23]. Calculated inter-planar spacings (d_{calc}, in Å) and unit-cell parameters are presented, as well.

MoPB			Re-MoPB			MoO_3[1]		
d_{obs}	d_{calc}	I_{obs}	d_{obs}	d_{calc}	I_{obs}	d_{obs}	I_{obs}	h k l
6.850	6.893	13	6.971	6.921	17	6.930	34	0 2 0
			4.884[#]		20			
3.773	3.787	43	3.798	3.802	52	3.810	82	1 1 0
3.445	3.446	26	3.447	3.460[R]	30	3.463	61	0 4 0
3.243	3.251	100	3.262	3.259	100	3.260	100	0 2 1
			3.188[#]		28			
2.989	2.990	4	3.008	3.002	5	3.006	13	1 3 0
			2.935[#]		4			
2.676	2.692[R]	6	2.685	2.699[R]	22	2.702	19	1 0 1
2.636	2.642	28	2.650	2.649	28	2.655	35	1 1 1
2.513	2.518	6	2.524	2.525	9	2.527	12	0 4 1
2.301	2.298	17	2.310	2.307	20	2.309	31	0 6 0
2.260	2.259	4				2.271	18	1 5 0
			2.047[#]		6			
1.968	1.969	11	1.976	1.977	16	1.982	13	2 0 0
1.952	1.949	10	1.958	1.957	10	1.960	17	2 1 0
			1.900[#]		6			
1.842	1.844	21	1.846	1.847	24	1.849	21	0 0 2
			1.736	1.729[R]	8	1.733	17	2 1 1
			1.734[#]		4			
			1.680[#]		5			
1.657	1.658	12	1.661	1.661	14	1.663	13	1 1 2
1.626	1.626	8	1.630	1.629	17	1.631	13	0 4 2
1.591	1.589	3	1.594	1.595	8	1.597	15	1 7 1
1.566	1.561[R]	8	1.568	1.567	8	1.569	16	0 8 1
			1.479	1.475[R]	4	1.477	10	2 5 1
1.439	1.438	7	1.442	1.442	8	1.443	12	0 6 2
1.426	1.428	3	1.432	1.433	7	1.435	12	1 9 0
1.347	1.346	5	1.350	1.350	4	1.352	6	2 0 2
a_0 (Å)	3.938(3)[*]		3.954(2)			3.962		
b_0 (Å)	13.786(9)		13.842(6)			13.85		
c_0 (Å)	3.687(2)		3.694(2)			3.697		
V_0 (Å^3)	200.2(2)		202.1(1)			202.99		

[1]Orthorhombic molybdite, MoO_3 [23]

[#]Tetragonal sodium perrhenate, $NaReO_4$ [22]

[R]Rejected from the calculations

[*]The numbers in parentheses are the esd's, and refer to the last significant number

Accepted Manuscript For Review Only

Table 2. Observed inter-planar spacings (d_{obs}, in Å) and intensities (I_{obs}, in %) of WPB and Re-WPB compared to the reference PW_8O_{26} with their adequate Miller's hkl indices presented [18]. Calculated inter-planar spacings (d_{calc}, in Å) and unit-cell parameters are also presented.

WPB			Re-WPB			PW_8O_{26}[1]		
d_{obs}	d_{calc}	I_{obs}	d_{obs}	d_{calc}	I_{obs}	d_{obs}	I_{obs}	h k l
			4.884[#]		10			
3.808	3.826	55	3.830	3.838	53	3.8395	41	0 0 2
3.738	3.753	100	3.754	3.758	100	3.7486	100	0 2 0
			3.188[#]		22			
3.079	3.081	6	3.097	3.079	5	3.0833	5	1 1 2
			2.935[#]		3			
2.667	2.675	61	2.676	2.680	65	2.6767	40	-2 0 2
						2.6373	26	2 0 2
			2.354[#]		6			
2.173	2.178	21	2.179	2.182	26	2.1732	14	-2 2 2
			2.047[#]		3			
			1.984	2.005[R]	18	2.0061	2	2 1 3
1.908	1.913	6	1.918	1.919	6	1.9218	3	0 0 4
			1.900[#]		7			
1.868	1.858	8	1.875	1.866	10	1.8657	11	-1 0 4
1.802	1.804	4	1.806	1.811	4	1.8095	4	-1 1 4
			1.740[#]		4			
1.702	1.704	11	1.706	1.709	12	1.7120	6	0 2 4
1.674	1.665	20	1.681	1.672	22	1.6685	15	-2 1 4
			1.628[#]		4			
			1.595	1.601	3	1.6033	1	2 3 3
1.549	1.555	8	1.552	1.560	7	1.5553	3	-2 2 4
1.533	1.529	10	1.534	1.529	11	1.5305	9	2 4 2
a_0 (Å)	7.39(9)[*]		7.35(8)			7.325(6)		
b_0 (Å)	7.51(4)		7.52(5)			7.516(9)		
c_0 (Å)	7.65(2)		7.68(2)			7.686(9)		
β (°)	90.8(4)		91.1(4)			90.79(5)		
V_0 (Å^3)	424(4)		424(3)			423.1(9)		

[1]Monoclinic PW_8O_{26} [18]

[#]Tetragonal sodium perrhenate, $NaReO_4$ [22]

[R]Rejected from the calculations

[*]The numbers in parentheses are the esd's, and refer to the last significant number

Accepted Manuscript For Review Only

Table 3. The electrochemical parameters obtained by fitting the EIS data recorded using the bronze-based electrodes in 0.5 M H_2SO_4

Electrode	R_{ct1}	Q_1 (μSs^{n1})	n1	R_s (Ω)	χ^2
MoPB	1190	4	0.7	27	0.093
MoPB-C	229	11	0.9	31	0.055
Re-MoPB	955	2	0.9	40	0.057
Re-MoPB-C	139	11	0.9	29	0.082
WPB	433	28	0.6	27	0.033
WPB-C	123	141	0.7	31	0.124

	R_{ct1} (Ω)	R_{ct2} (Ω)	Q_1 (μSs^{n1})	n1	Q_2 (μSs^{n2})	n2	R_s (Ω)	
Re-WPB	362	398	877	0.3	50.5	1.0	25	0.037
Re-WPB-C	50	89	530	0.6	812	0.8	29	0.066

Accepted Manuscript
For Review Only

Figure 1

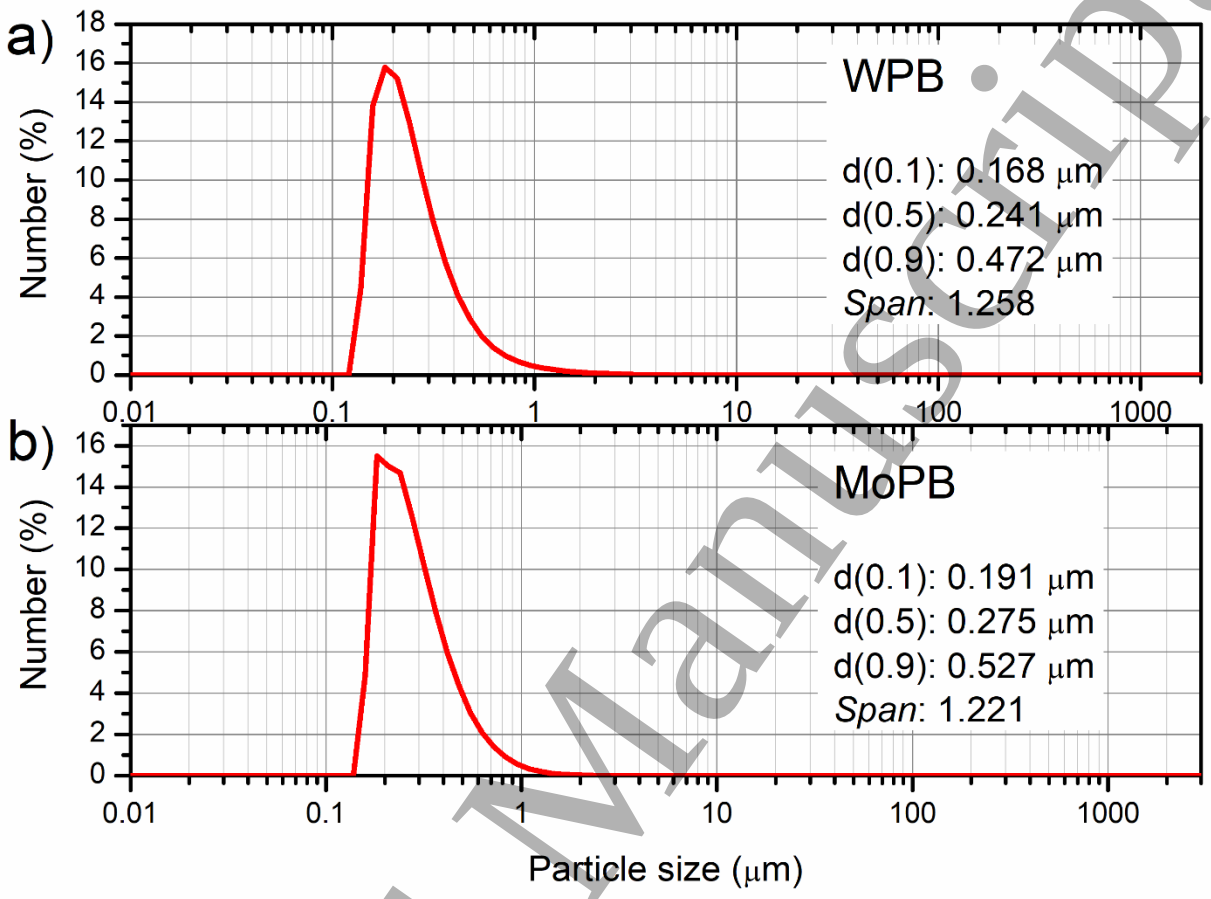

Accepted Manuscript Only

Figure 2

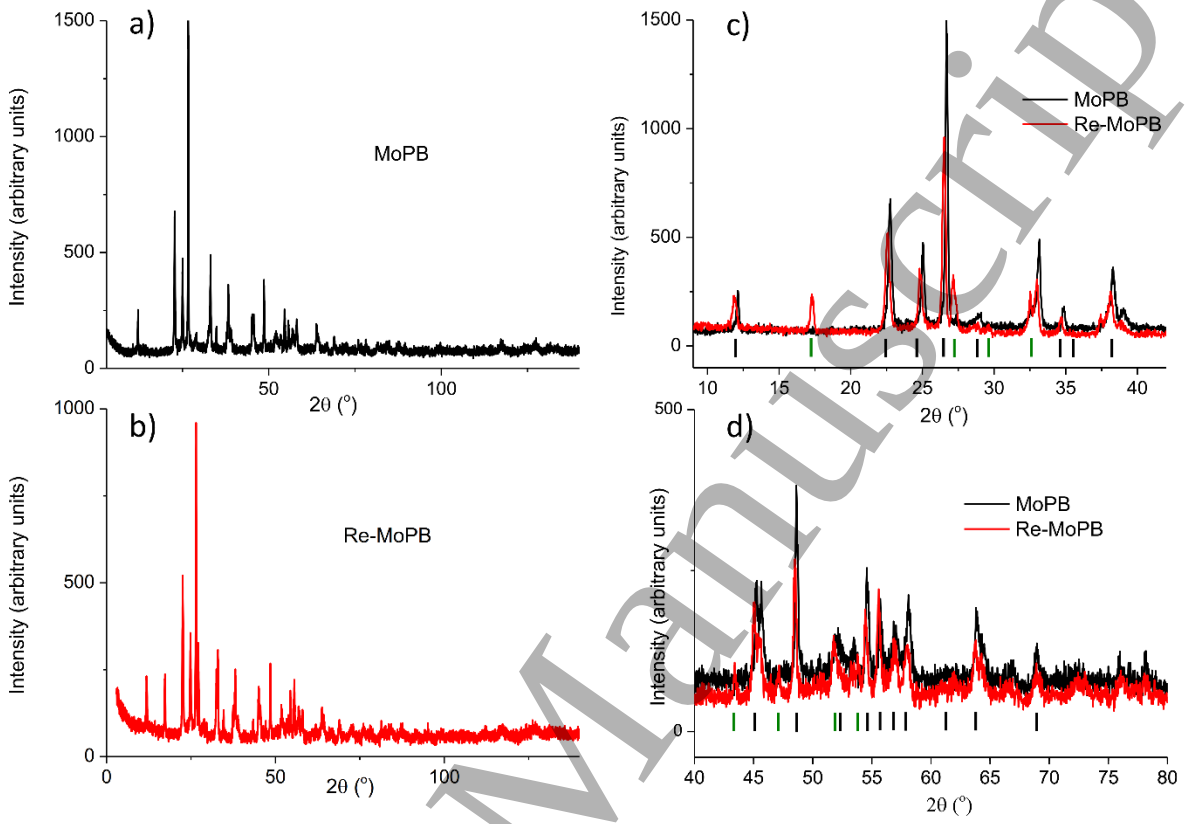

Accepted Manuscript
For Review Only

Figure 3

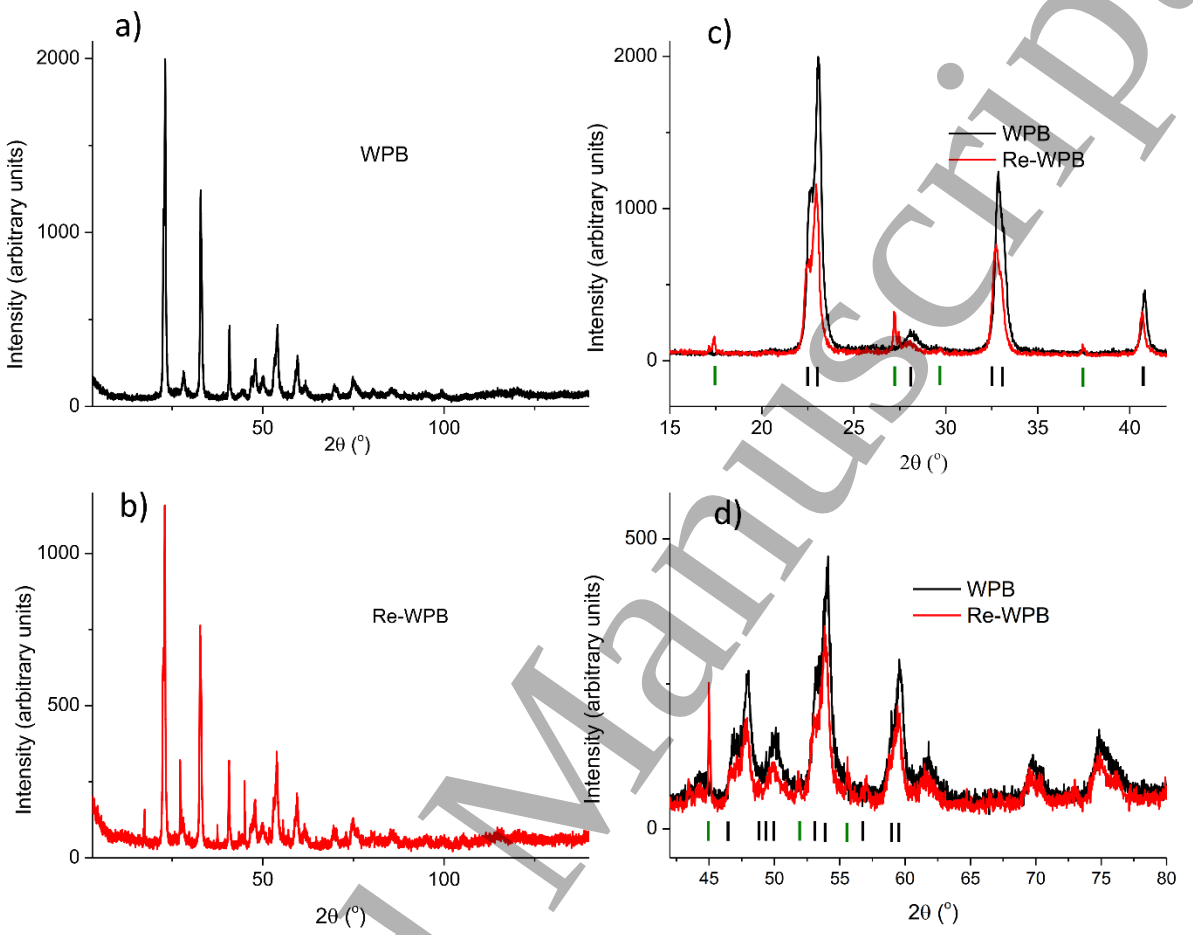

Accepted Manuscript

Figure 4

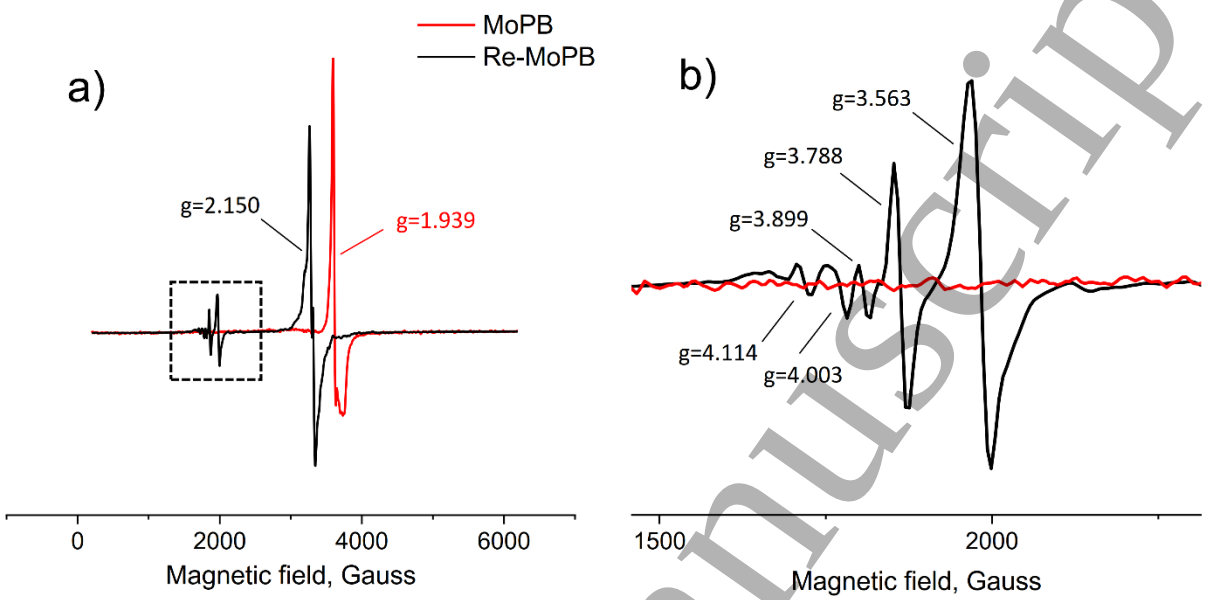

Accepted Manuscript
review Only

Figure 5

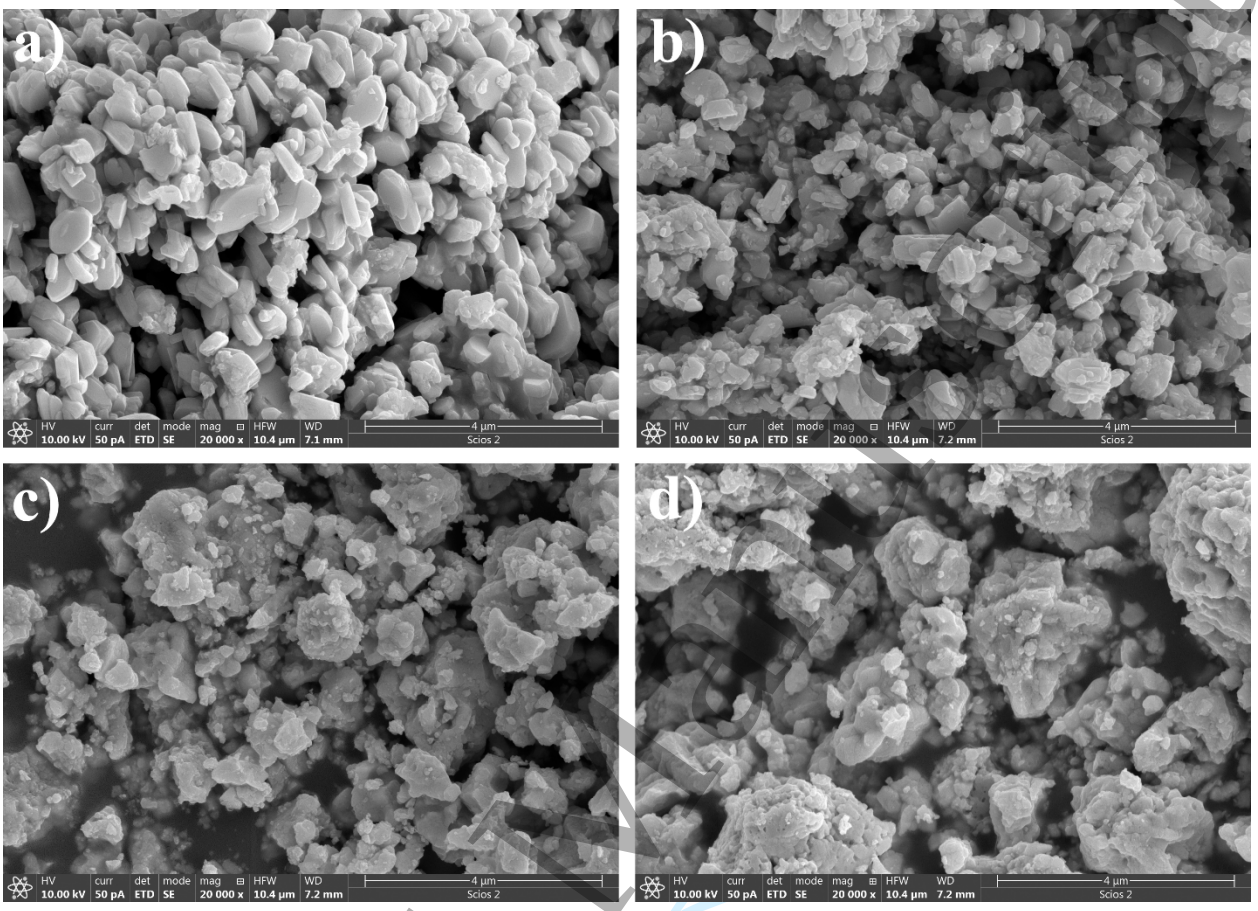

Accepted Manuscript

Figure 6

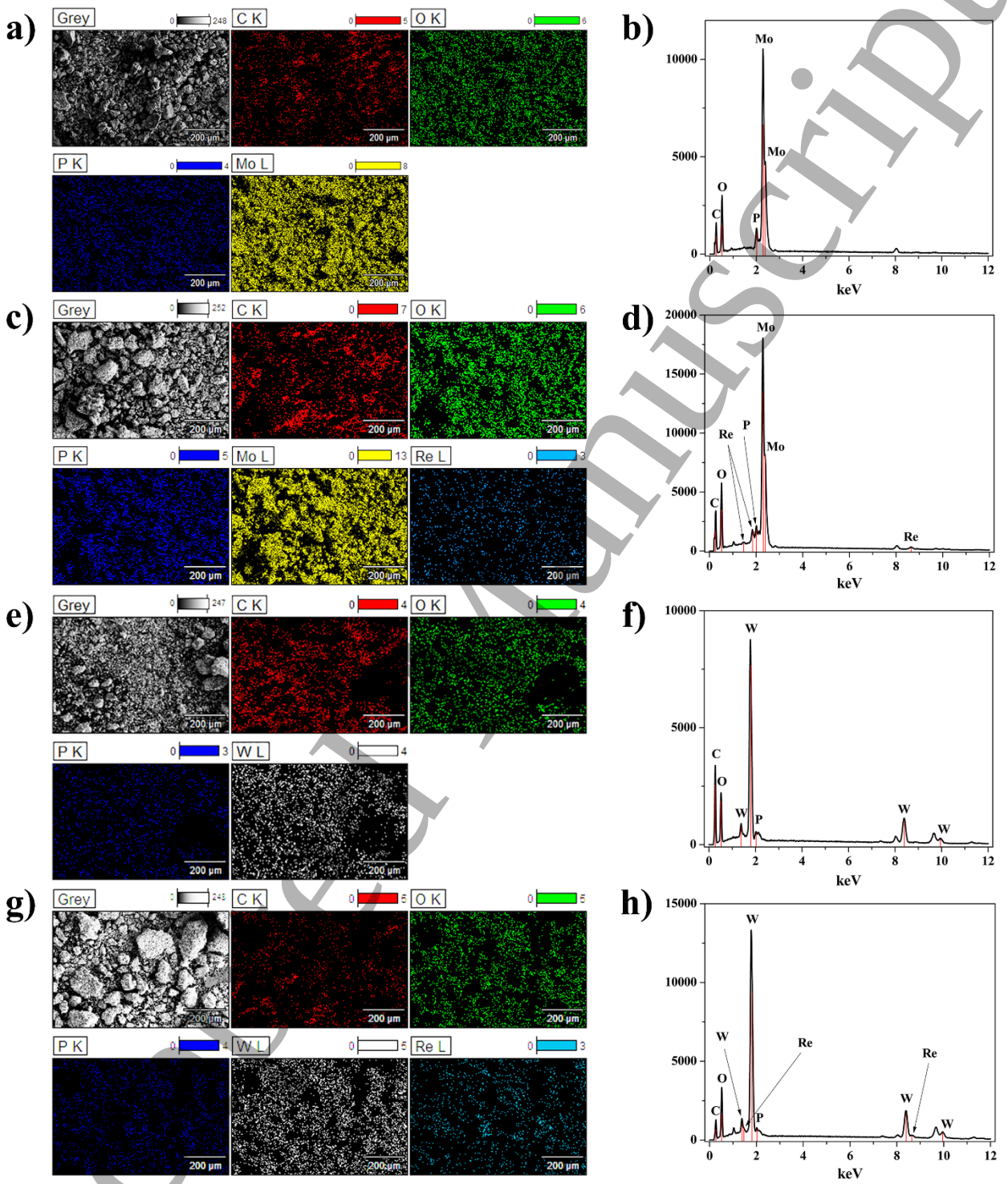

Accepted Manuscript

Figure 7

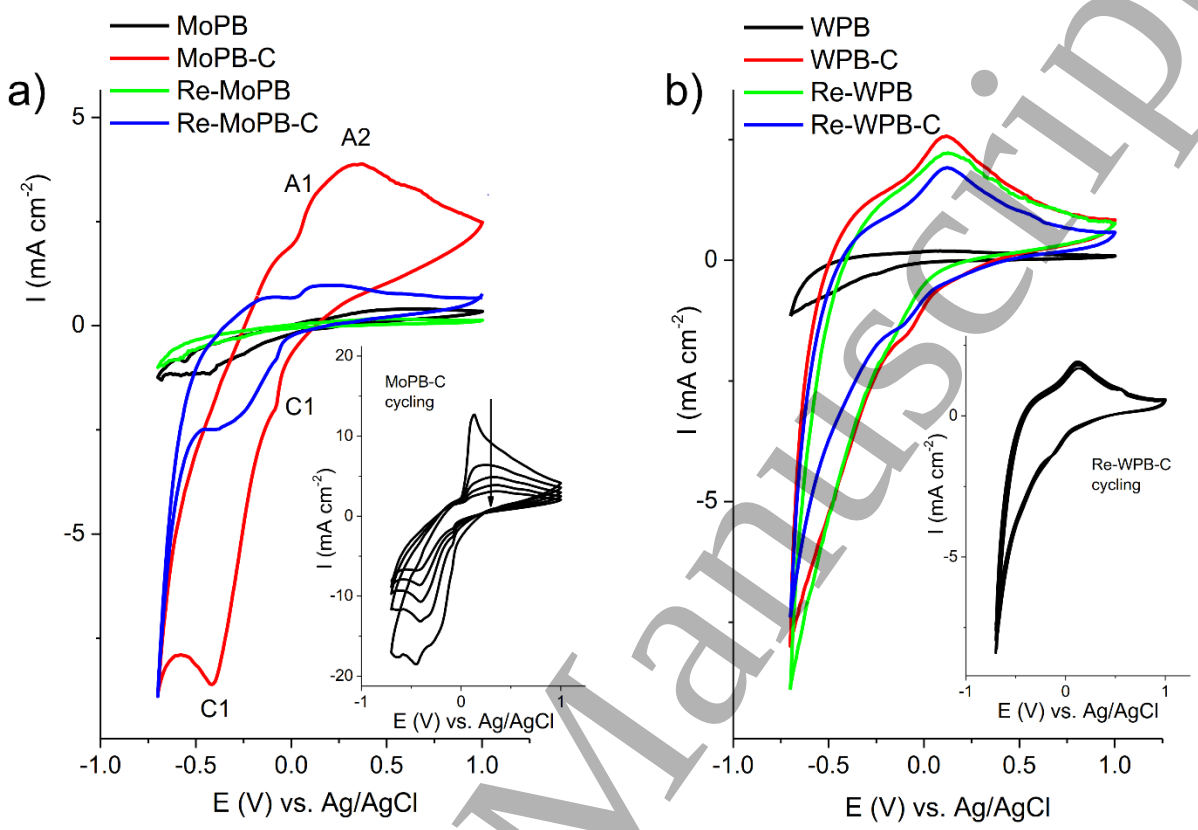

Accepted Manuscript
w Only

Figure 8

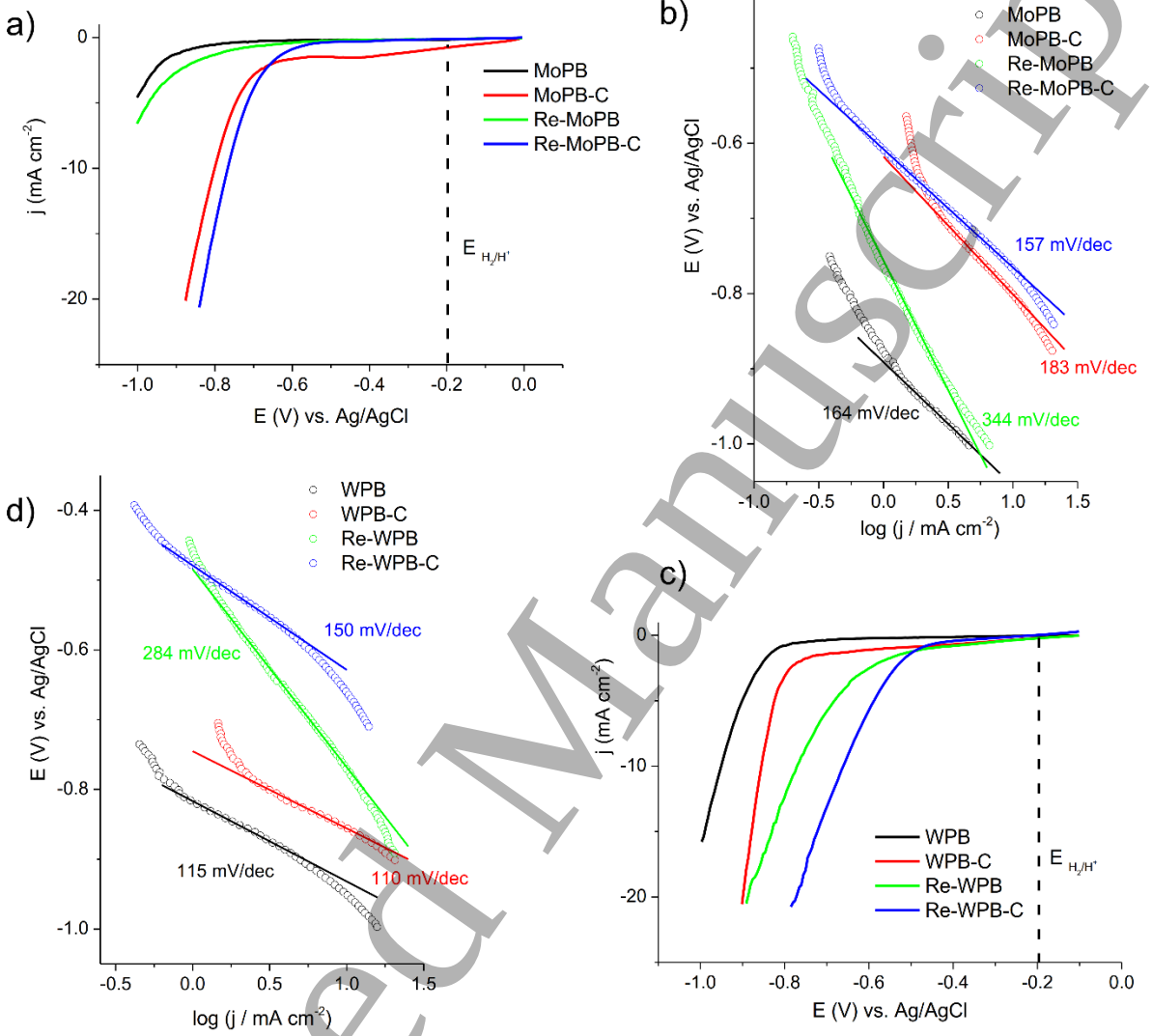

Accepted Manuscript

Figure 9

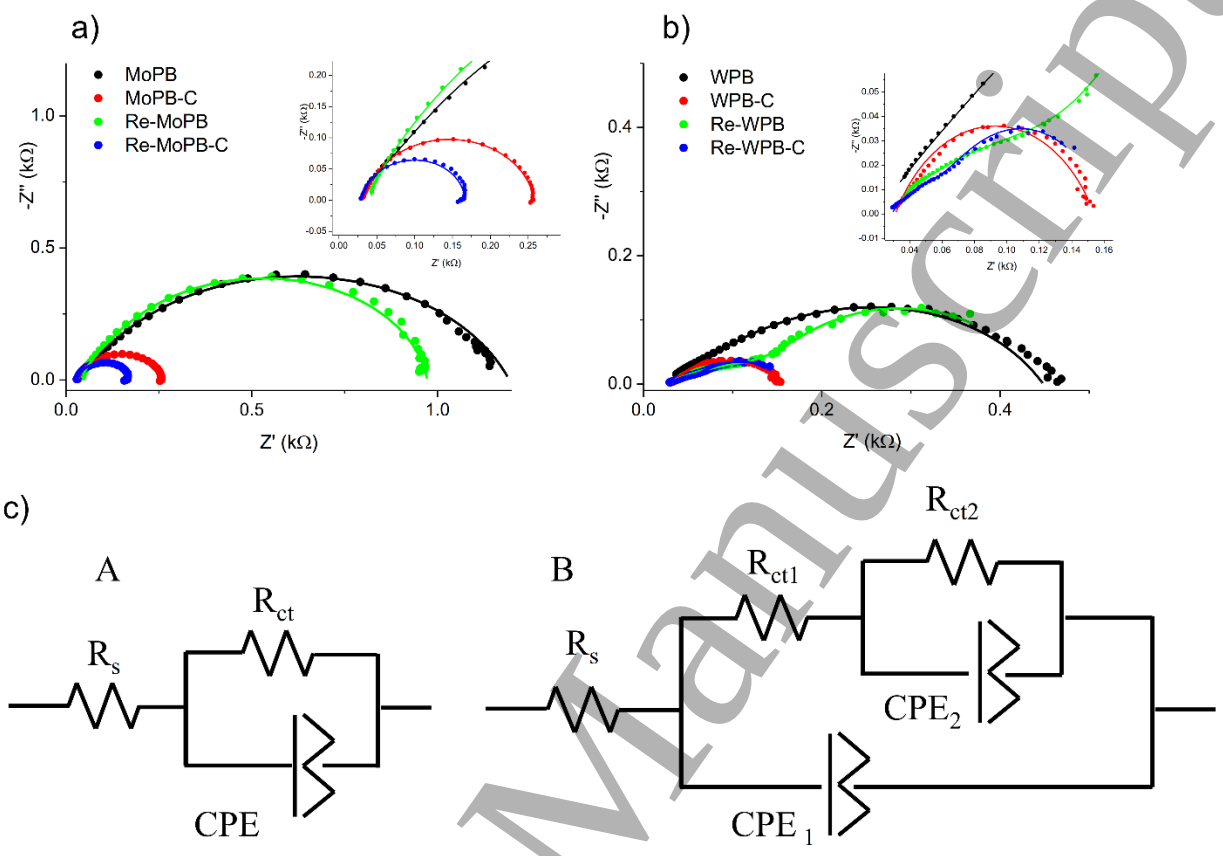

Accepted Manuscript
For Review Only